Modeling brine salinity from a proposed seawater desalination facility in Galveston Bay

Report prepared by
Jiabi Du, Ph.D.

Department of Marine and Coastal Environmental Sciences
College of Marine Sciences & Maritime Studies
Texas A&M University, Galveston, TX 77554

August 2025

Table of Contents

TABLE OF CONTENTS ..... **II**

LIST OF FIGURES/TABLES ..... **III**

PROJECT SUMMARY **1**

1. INTRODUCTION **3**

2. METHODS **4**

2.1 NUMERICAL MODEL 4

2.2 MODEL GRID 4

2.3 MODEL BATHYMETRY 8

2.4 MODEL INPUT FORCINGS 9

2.5 INTAKE AND DISCHARGE SALINITY 11

3 MODEL CALIBRATION **13**

3.1 WATER LEVEL 13

3.2 SALINITY 15

4. IMPACT OF BRINE DISCHARGE ON SALINITY **17**

4.1 LONG-TERM MEAN 17

4.2 TIME SERIES OVER DIFFERENT DISTANCES FROM THE DISCHARGE LOCATION 19

5. IMPACT OF BRINE DISCHARGE ON STRATIFICATION **25**

5.1 PERCENTAGE OF TIME WITH CONTINUOUS STRATIFICATION 25

5.2 TIME SERIES AT A SELECTED LOCATION 27

6. DISCUSSION AND SUMMARY **31**

REFERENCES **34**

List of Figures/Tables

Figure 1: (a) Horizontal model grid; (b) zoom-in view of the model grid for Galveston Bay, with blue dot indicating the intake location; (c) zoom-in view of the model grid near the bay mouth, with bathymetry indicated by color. 7

Figure 2: Zoom-in view of the model grid near the proposed desalination plant. Blue and red dots indicate the intake and discharge locations, respectively. 8

Figure 3: Nudging coefficient (filled color) within the nudging zone. Red open circles mark the open boundary nodes. 11

Figure 4: Intake (black) and outflow (red) salinity over the two-year period (2018–2019). Also shown is the modeled salinity at the tidal dam. The outflow salinity is calculated as 147% of the intake salinity. 13

Figure 5: Comparison of water levels between model results and observations. Mean absolute error (MAE), R^2, and root mean square error (RMSE) are shown at the top of each panel. Monitoring station locations are marked with magenta dots in the right subplots. Statistical metrics are based on the full two-year period (2018–2019), though only 25 days are shown in the plot. 14

Figure 6: Salinity comparison between model (red) and observation (black) at stations in Galveston Bay. Mean absolute error (MAE), R^2, and RMSE are shown at the top of each panel. Monitoring station locations are marked with magenta dots in the right subplots. 16

Figure 7: Two-year mean surface salinity from the base run (left panel) and scenario run (middle panel). The right panel shows the difference (scenario minus base), with positive values indicating salinity increase due to brine discharge. 17

Figure 8: Same as Figure 7, but showing a zoom-in view of salinity near the desalination plant. 18

Figure 9: Zoom-in view of the salinity difference (scenario minus base), same as the right panel of Figure 8 but using a different color scale. Differences smaller than 0.1 ppt are shown in white. The color interval is 0.5 ppt. Dashed curves indicate radii from 1 to 5 km centered at the tidal dam. 19

Figure 10: Regions within different radii (1–10 km) used for calculating regional mean salinity difference between the two model runs. 20

Figure 11: Time series of salinity difference (scenario minus base) averaged over different radii. Colored lines represent different averaging radii. Long-term mean differences are indicated by colored dots at the left of the plot. 21

Figure 12: Violin plot showing the distribution of regional mean salinity differences due to brine discharge. The white bar marks the median, the black rectangle shows the interquartile range, the vertical line indicates the full range, and the outer shape illustrates the data distribution. 22

Figure 13: Same as Figure 11, but for smaller averaging radii from 100 m to 1 km. 23

Figure 14: Same as Figure 12, but for smaller averaging radii from 100 m to 1 km. 23

FIGURE 15: LONG-TERM MEAN SALINITY DIFFERENCE AVERAGED OVER THE TWO-YEAR PERIOD AND OVER VARIOUS RADII. THE INSET AT TOP RIGHT SHOWS THE 1–5 KM RADII USED FOR REGIONAL AVERAGING. 24
FIGURE 16: PERCENTAGE OF TIME (%) WHEN BOTTOM–SURFACE SALINITY DIFFERENCE EXCEEDED 2 PPT FOR MORE THAN 24 HOURS. LEFT: BASE RUN; MIDDLE: SCENARIO RUN; RIGHT: DIFFERENCE BETWEEN THE TWO, WITH POSITIVE VALUES INDICATING A GREATER PERCENTAGE IN THE SCENARIO RUN. 26
FIGURE 17: SAME AS FIGURE 16, BUT SHOWING A ZOOM-IN VIEW NEAR THE DESALINATION PLANT. IN (A), THE CROSSES MARKS INDICATE FOUR SAMPLING LOCATIONS, AT 0.5 KM, 1 KM, 2 KM, AND 3 KM OFF THE TIDAL DAM. TIME SERIES OF BOTTOM-SURFACE SALINITY DIFFERENCE AT THESE TWO LOCATIONS ARE SHOWN IN FIGURE 18 AND FIGURE 21. 27
FIGURE 18: TIME SERIES OF BOTTOM–SURFACE SALINITY DIFFERENCE AT A SAMPLING LOCATION 0.5 KM OFFSHORE FROM THE TIDAL DAM NEAR THE DESALINATION PLANT. 29
FIGURE 19: TIME SERIES OF BOTTOM–SURFACE SALINITY DIFFERENCE AT A SAMPLING LOCATION 1 KM OFFSHORE FROM THE TIDAL DAM NEAR THE DESALINATION PLANT 29
FIGURE 20: TIME SERIES OF BOTTOM–SURFACE SALINITY DIFFERENCE AT A SAMPLING LOCATION 2 KM OFFSHORE FROM THE TIDAL DAM NEAR THE DESALINATION PLANT 30
FIGURE 21: TIME SERIES OF BOTTOM–SURFACE SALINITY DIFFERENCE AT A SAMPLING LOCATION 3 KM OFFSHORE FROM THE TIDAL DAM NEAR THE DESALINATION PLANT 30

Project Summary

Before developing the proposed Bayshore Desalination Facility in Texas City, Texas, EPCOR requested Texas A&M University at Galveston to assess the impact of brine water discharge on the salinity near the outflow location and of the entire Galveston Bay. Salinity is a fundamental water quality parameter that can determine how this project may impact the ecosystem.

Objective 1: Conduct numerical simulations for a base case (without brine discharge) and a scenario case (intake of 82.8 million gallons/day from Dickinson Bayou and discharge of 56.3 million gallons/day near Bayshore Park) using a reliable high-resolution ocean model to examine how salinity near the outflow area is affected.

Key Findings: Within 1 km of the tidal dam that connects the discharge channel to the bay, mean surface salinity increases by approximately 0.12 ppt, with the impact diminishing rapidly offshore. Within the discharge channel itself, salinity can increase by up to 5 ppt. The intake/discharge scheme can also be interpreted as a net reduction of approximately 26.5 MGD (or 1.39 m^3/s) of freshwater to the system. When compared to the total freshwater inflow into Galveston Bay—typically ~300 m^3/s from the San Jacinto River, Trinity River, and Buffalo Bayou (Marshall and Montagna, 2025)—this reduction is unlikely to significantly alter bay-wide salinity patterns.

A notable and somewhat unexpected finding is that the salinity impact is more pronounced near the intake channel (close to Dickinson Bayou) than near the discharge location, with salinity increasing by 0–1 ppt in Dickinson Bayou near the intake channel when averaged over a two-year simulation period (2018–2019). This is dynamically reasonable, as the intake channel acts as a sink, enhancing the landward movement of high-salinity seawater from the bay into Dickinson Bayou.

The salinity impact from brine discharge can also be negative, depending on the difference between the intake salinity and the ambient salinity at the discharge location. For example, when intake salinity is low (e.g., after a freshwater pulse into Dickinson Bayou), the discharged brine may be less saline than nearby bay water, thereby reducing salinity at the discharge site..

Objective 2: Examine how brine discharge will affect the salinity stratification and its potential impact on dissolved oxygen conditions.

Key Findings: Brine discharge can substantially increase the percentage of time with continuous stratification (defined as a surface–bottom salinity difference > 2 ppt sustained for over 24 hours) in the nearshore region. Within 1 km of the tidal dam, the percentage of time with continuous stratification can increase by up to 30%. This elevated stratification is primarily induced by density flow as denser brine water moves downslope along the bottom. However, the denser brine water also contains high levels of dissolved oxygen, making it unlikely that brine discharge will significantly impact the nearshore dissolved oxygen concentration. Similar to its effect on salinity, the impact of brine discharge on stratification decreases rapidly beyond 1 km from the tidal dam.

1. Introduction

EPCOR is conducting a development and feasibility assessment to potentially build and operate the Bayshore Desalination Facility in Texas City, TX. To evaluate the potential impacts of desalination on water quality and the ecosystem, EPCOR has requested Texas A&M University at Galveston (TAMUG) assess the effects of the proposed brine discharge on salinity levels near the desalination site and throughout the entire bay. Brine discharge is expected to influence salinity in the vicinity of the outfall location. The extent of this impact depends on the discharge rate, physical/thermodynamic characteristics of the brine, and how quickly it is diluted and dispersed into the surrounding coastal waters.

To accurately assess the effect of brine discharge on receiving waters, we used a well-calibrated hydrodynamic model (Du et al., 2019) and completed the following tasks:

1) Upgraded the model grid to better represent the seawater intake channel and the shoreline near the discharge location.
2) Validated the model by comparing the baseline simulation (without brine discharge) to observations of water level and salinity.
3) Conducted a scenario simulation that included an intake of 82.8 million gallons per day and a discharge of 56.3 million gallons per day of diluted brine.
4) Analyzed the differences between the baseline and scenario simulations, focusing on changes in salinity near the discharge site and across the bay.
5) Assessed the impact of brine discharge on salinity stratification, specifically the frequency and duration of events where the bottom-to-surface salinity difference exceeds 2 ppt for more than 24 hours.

In this report, we describe the model setup, demonstrate its reliability, and present results on the salinity impacts of the proposed brine discharge.

2. Methods

2.1 Numerical model

In this study, we employed the **S**emi-implicit **C**ross-scale **H**ydroscience **I**ntegrated **S**ystem **M**odel (SCHISM; Zhang et al., 2015, 2016), an open-source, community-supported modeling system based on unstructured grids and derived from the earlier SELFE model (Zhang and Baptista, 2008). SCHISM uses a highly efficient semi-implicit finite-element/finite-volume method with a Eulerian–Lagrangian algorithm to solve the turbulence-averaged Navier–Stokes equations under the hydrostatic and Boussinesq approximations. For turbulence closure, it uses the generic length-scale model of Umlauf and Burchard (2003) along with the stability function of Kantha and Clayson (1994). One of the major advantages of SCHISM is its flexible vertical grid system, which robustly and accurately resolves complex topography in estuarine and oceanic systems without the need for smoothing (Zhang et al., 2016; Du et al., 2018; Ye et al., 2018).

The model has been applied globally (see examples at: https://ccrm.vims.edu/schismweb/). The modeling team at TAMUG has been developing model applications for the northern Gulf of Mexico since 2017 and has validated and applied the model in multiple studies (Du et al., 2019; Du and Park, 2019; Du et al., 2020; Summers et al., 2023; Hua et al., 2025). SCHISM has demonstrated high reliability in simulating water level, salinity, temperature, and ocean circulation in coastal bays and across the Texas–Louisiana shelf under both typical conditions and extreme weather events. Recently, the model has also been adopted by the Texas Water Development Board for short-term forecasting in their daily operation (https://midgewater.twdb.texas.gov/index.html).

2.2 Model grid

The hydrodynamic model used in this study is largely based on the configuration presented in Du et al. (2019), where the model domain covers the entire Texas, Louisiana, Mississippi, and Alabama coasts (Fig. 1a). However, the original setup lacked fine resolution for coastal bays other than Galveston Bay. To address this limitation, we upgraded the model mesh by:

1) Resolving geometric and bathymetric features such as deep and narrow ship channels present in all major coastal bays along the northern Gulf of Mexico;
2) Extending the model domain approximately 100 km farther south (the previous southern boundary was near the U.S.–Mexico border);
3) Refining the resolution in the deep Gulf from 10 km to 5 km to better capture shelf-wide circulations (Hua et al., 2025); and
4) Including additional coastal bays, such as Perdido and Pensacola bays in the Florida Panhandle.

Mesh resolution was improved for all 13 major coastal bays, including (from west to east): Lower Laguna Madre, Upper Laguna Madre, Corpus Christi Bay, Mission–Aransas Estuary, San Antonio Bay, Matagorda Bay, East Matagorda Bay, Galveston Bay, Sabine Lake, Calcasieu Lake, Mobile Bay, Perdido Bay, and Pensacola Bay (Fig. 1a). The grid resolution ranges from 10 meters in small creeks and tidal channels to an average of 2.5 km over the continental shelf and 5 km in the open ocean.

For Galveston Bay, the model grid accurately resolves ship channels and major rivers (Fig. 1b, 1c). A hybrid grid, combining rectangular and triangular elements, was used to enhance computational performance and more accurately represent salt transport along major channels. Well resolving the deep but narrow ship channel is vitally important for salt intrusion simulation.

To examine the impact of brine discharge from the proposed desalination facility, we further refined the grid by:

1) Explicitly resolving the intake and discharge channels near the desalination facility; and
2) Reducing grid size in the vicinity of the intake and discharge points (Fig. 2). Finer resolution near the discharge location ensures smoother transitions between small grids in the channels and coarser grids along the bay's shoreline, improving the simulation of salinity in that region.

The updated model grid consists of 129,157 grid nodes and 214,080 grid elements. An *element* refers to a basic computational unit (e.g., a triangle or rectangle) over which governing equations

(e.g., for fluid flow, temperature, or salinity) are solved. *Grid nodes* are the vertices that define the boundaries of these elements.

Vertically, we implemented the Localized Sigma Coordinates with Shaved Cells (LSC^2), a hybrid vertical coordinate system, instead of the hybrid s–z grid used in Du et al. (2019). Unlike traditional sigma grids, which use a fixed number of layers regardless of depth, LSC^2 dynamically adjusts the number of layers based on local bathymetry. This leads to improved computational efficiency, especially in coastal systems with extensive shallow regions (Zhang et al., 2015; Ye et al., 2020). LSC^2 is particularly effective in handling sharp bathymetric features, such as the narrow (~100–200 m wide) but deep (~15 m) ship channels common in northern Gulf coastal bays. For example, in the Houston Ship Channel, the model includes approximately 27 vertical layers, while in shallow shoals, it uses about 10 layers.

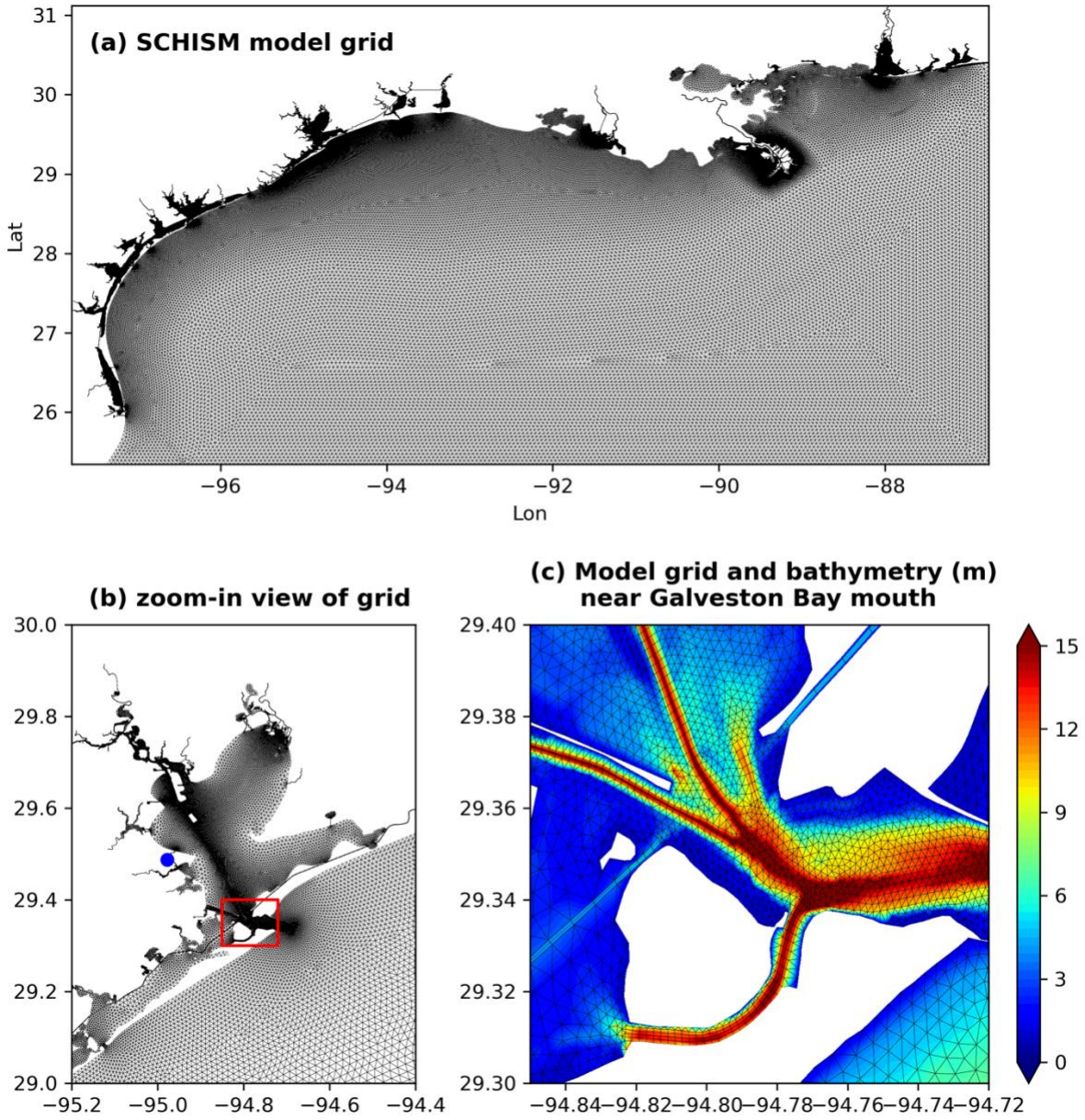


Figure 1: (a) Horizontal model grid; (b) zoom-in view of the model grid for Galveston Bay, with blue dot indicating the intake location; (c) zoom-in view of the model grid near the bay mouth, with bathymetry indicated by color.

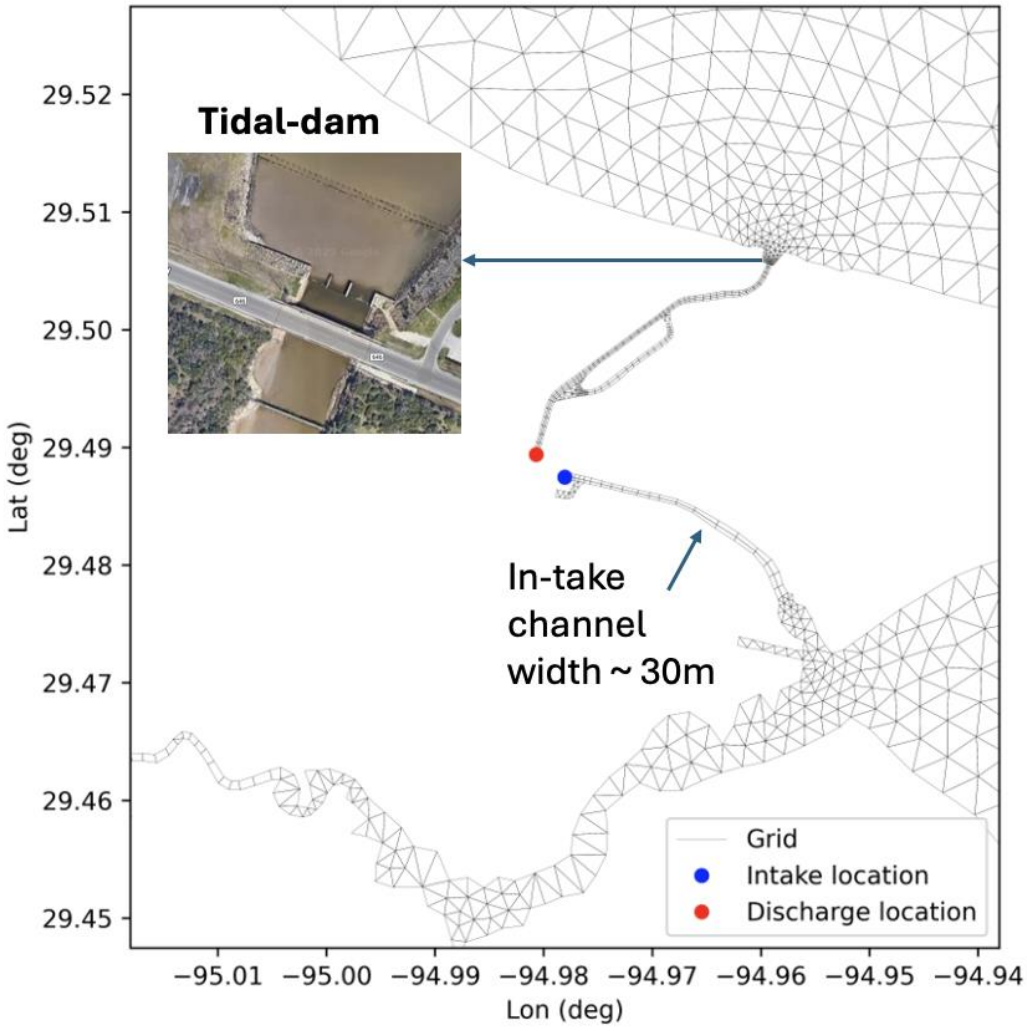


Figure 2: Zoom-in view of the model grid near the proposed desalination plant. Blue and red dots indicate the intake and discharge locations, respectively.

2.3 Model bathymetry

Bathymetric data from two primary sources were used: ETOPO1 (1 arc-minute global relief model, developed by the National Geophysical Data Center; https://www.ncei.noaa.gov/products/etopo-global-relief-model) and CUDEM (1/9 arc-second Continuously Updated Digital Elevation Model, maintained by NOAA; https://chs.coast.noaa.gov/htdata/raster2/elevation/NCEI_ninth_Topobathy_2014_8483).

ETOPO1 is primarily used for representing the continental shelf and deep Gulf, while CUDEM, with its finer resolution (~3 meters), is employed in nearshore areas and coastal bays. The high resolution of CUDEM allows the model to resolve fine-scale bathymetric features, including narrow ship channels.

2.4 Model input forcings

To drive the model, several input forcings are incorporated, including: 1) freshwater discharge at major rivers; 2) atmospheric forcings, such as solar radiation, precipitation, wind, air temperature, and surface pressure; and 3) open boundary conditions for water level, temperature, salinity, and velocity along the southern and eastern boundaries of the model domain.

River discharge at 29 locations is derived from USGS gauging data. The river names and discharge locations are provided in Table 1. For Galveston Bay, the major contributing rivers include Buffalo Bayou, Chocolate Bayou, San Jacinto River, Trinity River, Clear Creek, and Dickinson Bayou.

Atmospheric forcing is derived from the North American Regional Reanalysis (NARR; https://psl.noaa.gov/data/gridded/data.narr.html) produced by the National Centers for Environmental Prediction (NCEP). NARR provides data at ~32 km spatial resolution with a 3-hour temporal interval.

At the open boundary, water level is specified separately for tidal and subtidal components. The tidal component is derived from the global tidal product FES2014 (Carrere et al., 2015) and includes eight tidal constituents: O1, K1, Q1, P1, M2, S2, K2, and N2. Among these, the diurnal tides (O1 and K1) are dominant in the model domain, with significantly larger amplitudes compared to semidiurnal constituents (M2 and S2). The subtidal component is derived from a low-pass filtered version (with a cutoff period of 50 hours) of the HYCOM 3-hourly global water level product (https://www.hycom.org). Although the northern Gulf is generally classified as a microtidal regime, tides still play a critical role in estuarine transport and mixing processes.

Subtidal temperature, salinity, and velocity are also specified at the open boundary using HYCOM output. In addition, a temperature and salinity nudging scheme is applied along the

boundary to prevent the model from drifting away from prescribed values (Chen et al., 2013). Nudging is particularly useful for stabilizing boundary zones and ensuring consistency when waves or flow propagate outward from the region of interest. A ~50 km-wide nudging zone is used, with stronger nudging (i.e., faster adjustment) closer to the boundary (see Fig. 3).

Table 1: Freshwater input locations at major rivers included in the model.

NO.	River Name	Lon	Lat
1	San Fernando Creek	-97.773	27.401
2	Nueces River	-97.605	27.869
3	Rio Grande	-97.290	25.936
4	Aransas River	-97.284	28.095
5	Mission River	-97.196	28.186
6	Guadalupe River	-96.842	28.468
7	Lavaca River	-96.576	28.870
8	Carancahua Creek	-96.422	28.772
9	Tres Palacios River	-96.147	28.812
10	Colorado River	-96.035	28.862
11	Caney Creek	-95.670	28.829
12	San Bernard River	-95.557	28.951
13	Brazos River	-95.530	29.036
14	Buffalo Bayou	-95.355	29.762
15	Chocolate Bayou	-95.229	29.260
16	San Jancinto River	-95.131	29.918
17	Clear Creek	-95.179	29.520
18	Dickinson Bayou	-95.102	29.430
19	Trinity River	-94.745	29.877
20	Neches River	-94.087	30.103
21	Sabine River	-93.702	30.114
22	Calcasieu River	-93.284	30.200
23	Atchafalaya River	-91.490	30.040
24	Mississippi River	-91.198	30.491
25	Pearl River	-89.638	30.287
26	Alabama River	-87.952	31.115
27	Tombigbee River	-87.952	31.115
28	Fish River	-87.810	30.443
29	Bon Secour River	-87.709	30.319

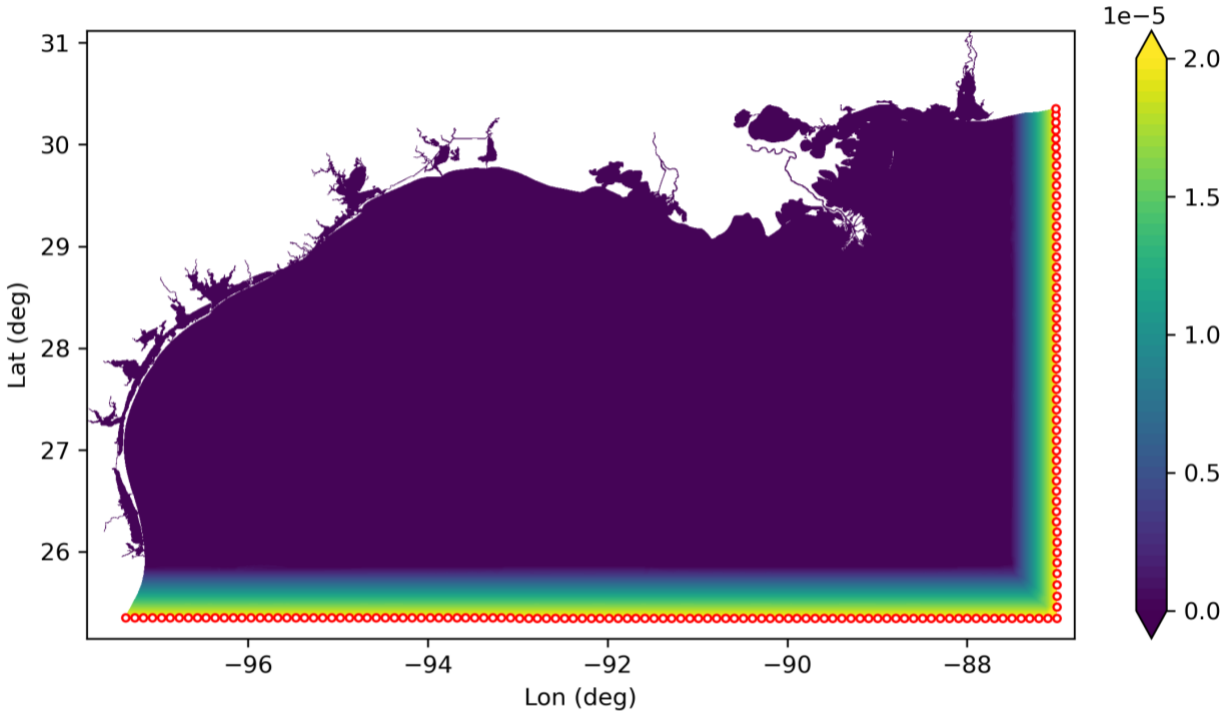


Figure 3: Nudging coefficient (filled color) within the nudging zone. Red open circles mark the open boundary nodes.

2.5 Intake and discharge salinity

After upgrading the model grid, we conducted a base model run covering the period from 2018 to 2019. We chose 2018-2019 because the modelled salinity has been well validated throughout the Galveston Bay for these two years (see model validations in Section 3 and in previous studies including Summers et al., 2024 and Hua et al., 2025). This base run did not include seawater intake or brine water discharge. We extracted salinity values near the proposed intake location. Salinity at the intake location ranged from a maximum of 22 ppt in the summer of 2018 to nearly 0 ppt in May 2019 (approximately day 500 since January 1, 2018; see Fig. 4). These variations were primarily driven by freshwater inflow and wind-driven circulation patterns in the bay and on the shelf. This wide range of salinity provides a valuable opportunity to evaluate the impact of brine discharge under diverse environmental conditions.

Based on the intake salinity, we calculated the salinity of the brine discharge (i.e., the outflow salinity) using a salt balance approach:

$$S_{in}F_{in} = S_{out}F_{out} \quad (1)$$

Or

$$S_{out} = S_{in}\frac{F_{in}}{F_{out}} \quad (2)$$

Where S_{in} is the intake salinity, S_{out} is the outflow (brine) salinity, F_{in} is the intake flow rate, and F_{out} is the outflow rate.

Given a constant intake flow of 82.8 million gallons per day (MGD) and an outflow rate of 56.3 MGD, the outflow salinity is approximately 147% of the intake salinity. Consequently, the brine salinity varies over time and is in phase with the intake salinity. The maximum difference between intake and brine salinity occurs during the summer of 2018, reaching approximately 10 ppt.

We also examined the ambient salinity near the outflow location (green line in Fig. 4) and noted that the brine water salinity could be occasionally smaller than the ambient salinity near outflow location (e.g., around day 340, 500, 620).

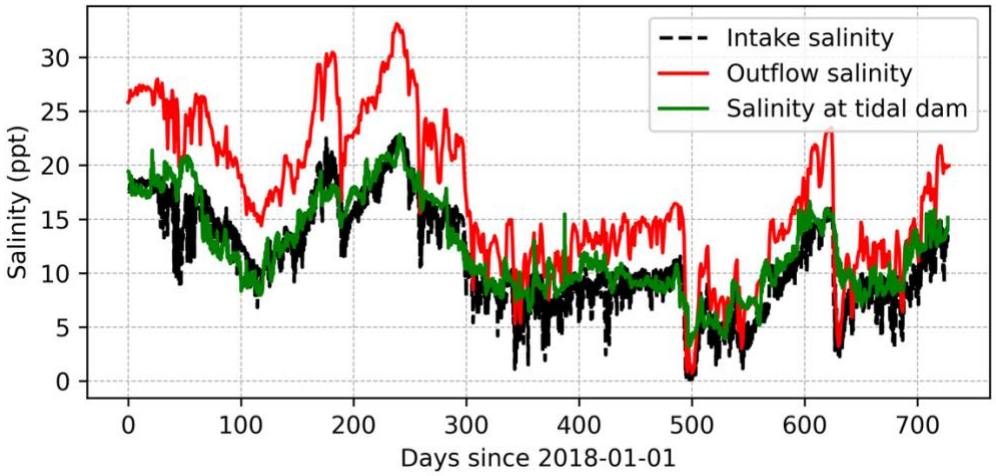


Figure 4: Intake (black) and outflow (red) salinity over the two-year period (2018–2019). Also shown is the modeled salinity at the tidal dam. The outflow salinity is calculated as 147% of the intake salinity.

3 Model calibration

Before applying the model for any numerical experiments, we conducted a thorough validation by comparing model results with observed ocean data to ensure the model accurately reproduces real-world conditions. While model validation has been presented in previous studies (Du et al., 2019; Du and Park, 2019; Summers et al., 2023; Summers et al., 2024; Hua et al., 2025), updates to the model grid—especially improvements to the resolution near the seawater intake and brine discharge channels—necessitate re-evaluation. Below, we present validation results for both water level and salinity within Galveston Bay.

3.1 Water level

Comparisons between modeled and observed water levels at two stations within the bay demonstrate strong model performance. The mean absolute error (MAE) is 0.05 m at both the bay mouth and upper bay stations (Fig. 5). The root mean square error (RMSE) is 0.07 m and 0.06 m, respectively. In coastal ocean modeling, an RMSE below 0.10 m is generally considered indicative of good model performance.

At both stations, the model effectively captures both tidal and subtidal components of water level. Despite the relatively short distance between the bay mouth and upper bay, water levels exhibit spatial variability. Notably, the upper bay station displays distinctly different subtidal variations. For example, around day 42, the upper bay experienced a more pronounced drop in water level compared to the bay mouth, likely due to wind-driven processes. The model's ability to reproduce these differences suggests that both the hydrodynamic model and the atmospheric forcing data are reliable.

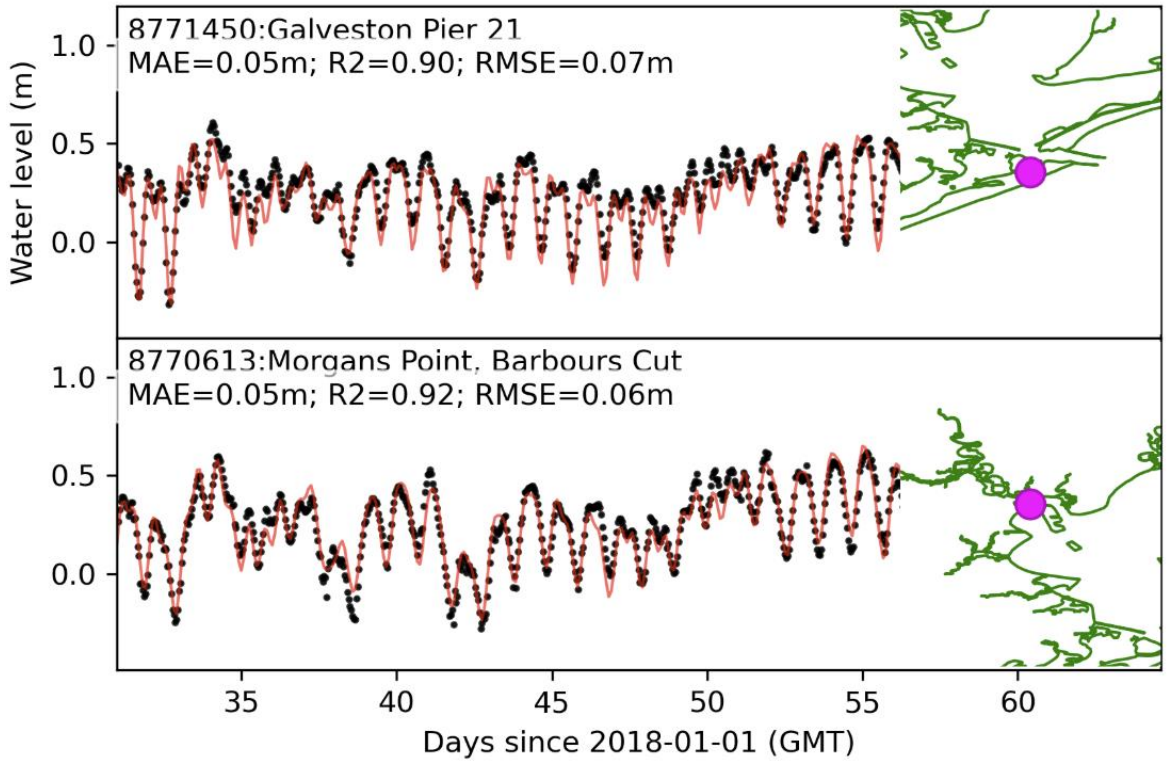


Figure 5: Comparison of water levels between model results and observations. Mean absolute error (MAE), R^2, and root mean square error (RMSE) are shown at the top of each panel. Monitoring station locations are marked with magenta dots in the right subplots. Statistical metrics are based on the full two-year period (2018–2019), though only 25 days are shown in the plot.

3.2 Salinity

Salinity is one of the most critical variables in hydrodynamic modeling of coastal systems. Accurate salinity simulation reflects the model's capability to capture physical transport processes, which are influenced by advection, diffusion, mixing, freshwater inflows, and coastal ocean dynamics.

The model performs particularly well in Galveston Bay (Fig. 6). The mean absolute error in salinity is 2–3 ppt across multiple stations with long-term, high-quality hourly observational data. At the bay mouth, the model accurately reproduces strong salinity variations influenced by both local freshwater inflow and remote freshwater transport along the coast, notably from the Mississippi and Atchafalaya Rivers (Du et al., 2019).

The model also successfully replicates spatial differences in the strength of tidal salinity signals across the bay. Tidal salinity variability is strongest at the bay mouth, weaker in the middle bay, and minimal to negligible in Trinity Bay. This gradient reflects both the salinity distribution and the efficiency of water exchange, with the bay mouth known to have more vigorous tidal exchange compared to the upper bay and Trinity Bay.

In summary, the model demonstrates reliable performance in simulating spatial salinity gradients, temporal variability, and regional differences in tidal influence across Galveston Bay.

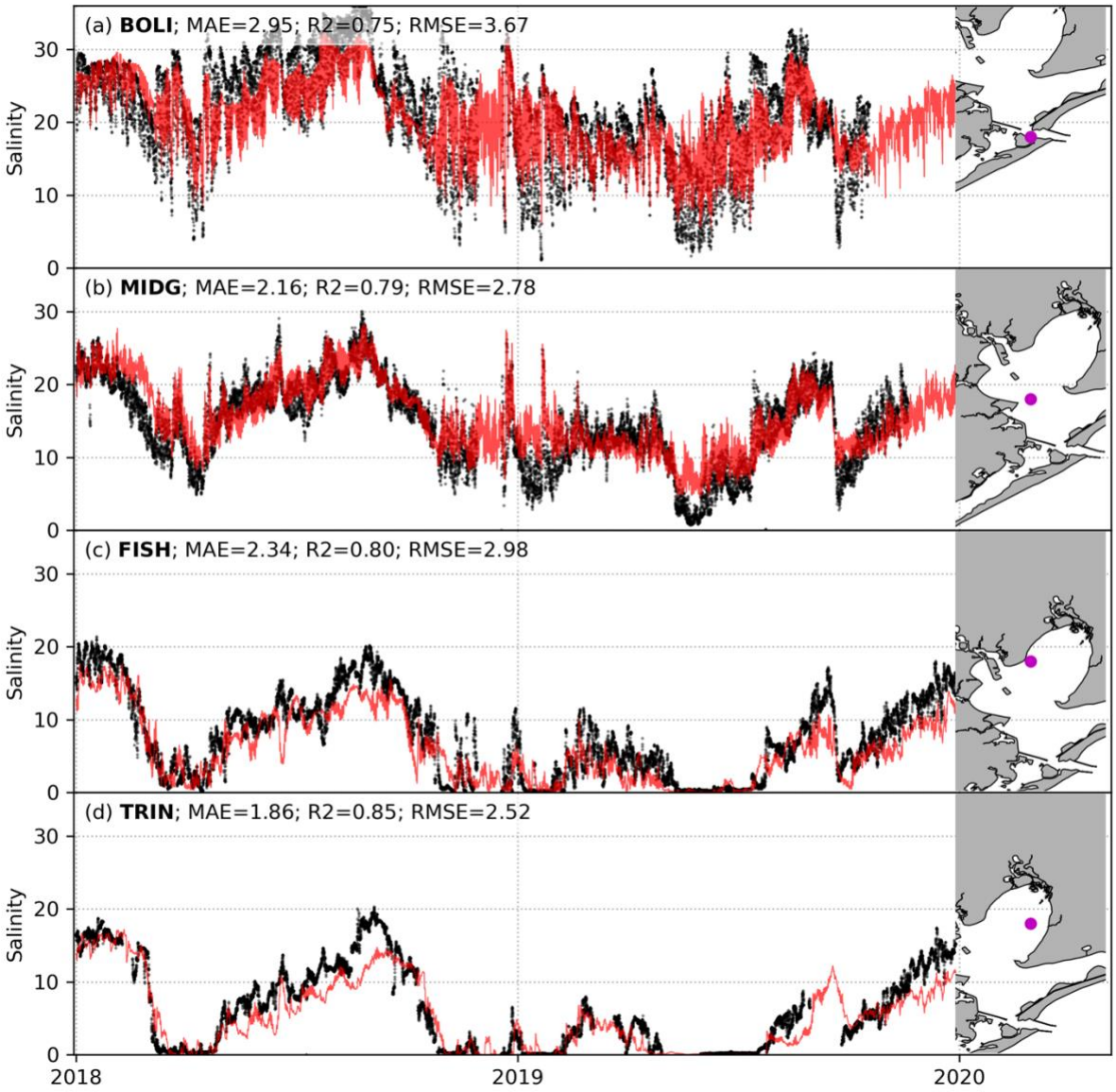


Figure 6: Salinity comparison between model (red) and observation (black) at stations in Galveston Bay. Mean absolute error (MAE), R^2, and RMSE are shown at the top of each panel. Monitoring station locations are marked with magenta dots in the right subplots.

4. Impact of brine discharge on salinity

4.1 Long-term mean

A comparison between surface salinity in the base run and the scenario run (with brine discharge) shows that the impact of brine discharge is most pronounced near the intake and discharge channels (Fig. 7). In other areas of the bay (e.g., Trinity Bay, Upper Galveston Bay, East Bay), the salinity increases slightly—by less than 1 ppt. In contrast, salinity slightly decreases in lower Galveston Bay and in the adjacent inner shelf ocean.

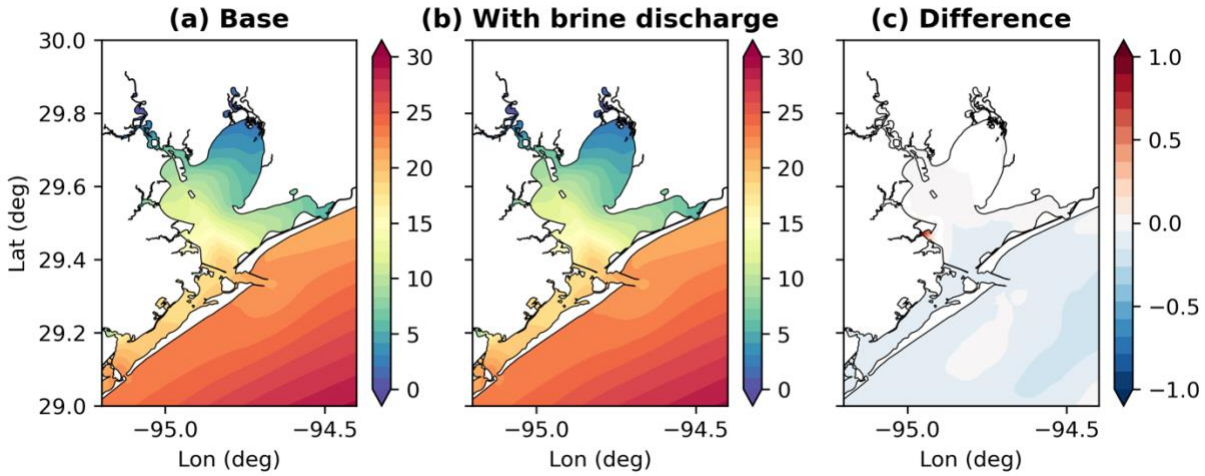


Figure 7: Two-year mean surface salinity from the base run (left panel) and scenario run (middle panel). The right panel shows the difference (scenario minus base), with positive values indicating salinity increase due to brine discharge.

Zooming into the area around the proposed desalination plant (Fig. 8), salinity increases are observed near the tidal dam, with the impact diminishing quickly offshore. A noticeable increase (greater than 0.1 ppt) is confined to a 7 km (along the shore) × 1 km (toward offshore) region around the tidal dam. The impact area extends more toward the northwest than the southeast. Interestingly, the increase is stronger near the intake channel (close to Dickinson Bayou), where salinity increases by at least 0.1 ppt along the entire ~10 km length of the bayou. Within the intake channel itself, salinity increases exceed 1 ppt.

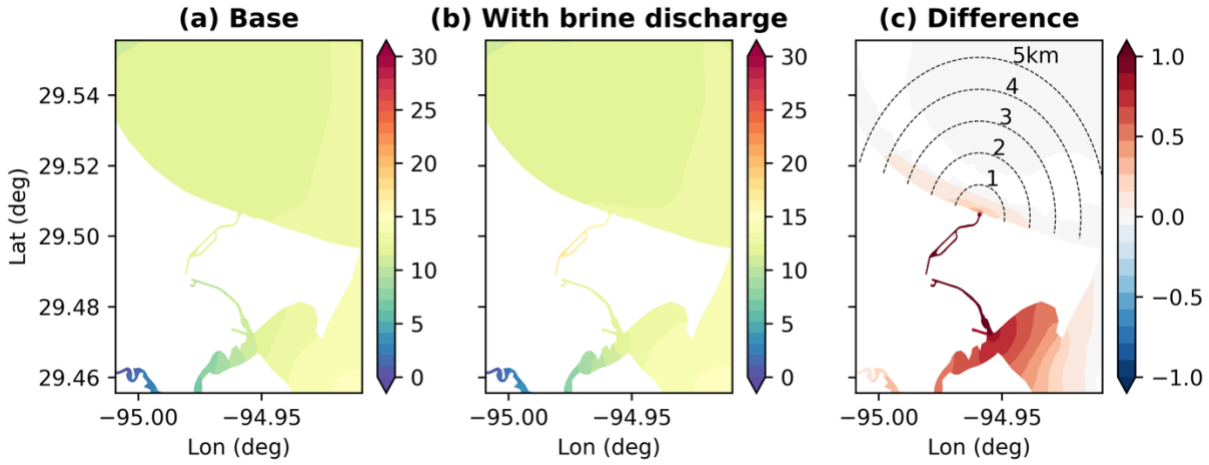


Figure 8: Same as Figure 7 but showing a zoomed-in view of salinity near the desalination plant.

However, the greatest salinity change occurs in the discharge channel, where increases reach up to 5 ppt (Fig. 9), compared to a maximum increase of ~2 ppt in the intake channel. Brine discharged from the proposed desalination plant is rapidly diluted by the larger volume of bay water, resulting in a sharp decline in the salinity impact offshore.

The increase in salinity near the intake channel is due to the water loss caused by the intake mechanism, which behaves like a “sinkhole” drawing in seawater. This promotes increased seawater intrusion into Dickinson Bayou to compensate for the withdrawal, thereby raising salinity. The impact region is larger near the intake channel than near the discharge channel, likely due to the restricted geometry of the bayou compared to the more open outflow area.

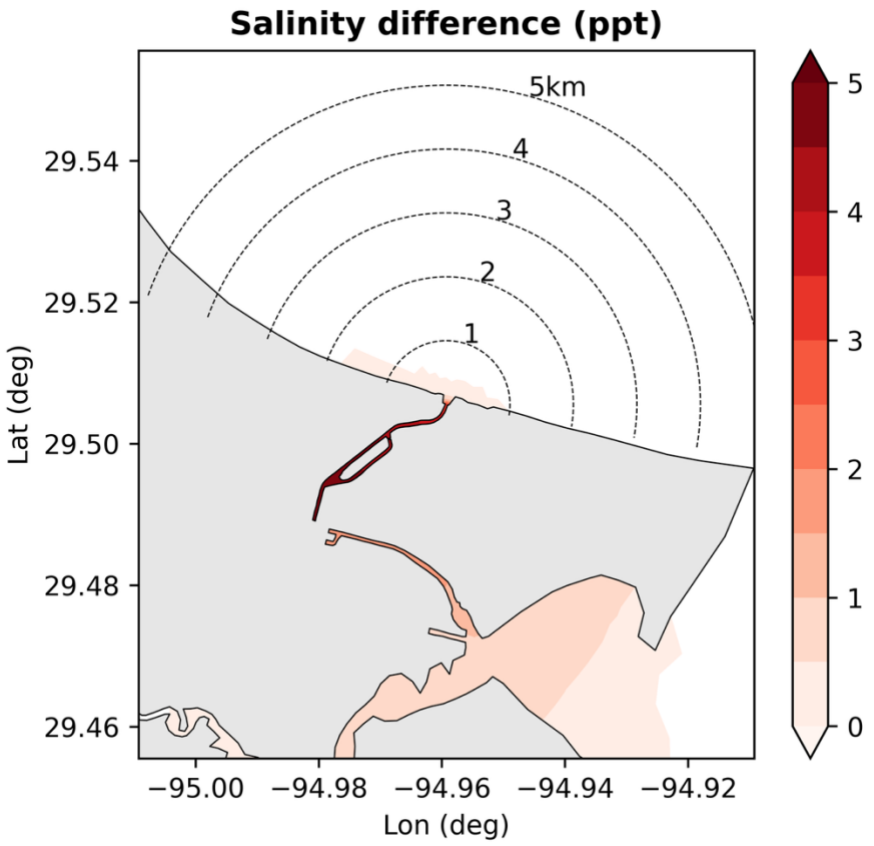


Figure 9: Zoom-in view of the salinity difference (scenario minus base), same as the right panel of Figure 8 but using a different color scale. Differences smaller than 0.1 ppt are shown in white. The color interval is 0.5 ppt. Dashed curves indicate radii from 1 to 5 km centered at the tidal dam.

4.2 Time series over different distances from the discharge location

To further assess the temporal behavior of salinity impact, we examined the time series of salinity differences (scenario run minus base run) averaged over different radii (1–10 km) from the tidal dam (i.e., mouth of the outflow channel). As illustrated in Fig. 10, we excluded the discharge channel from the analysis to focus on offshore impacts. For each day and radius, we computed the daily mean salinity difference and then averaged it over the given area. The resulting time series for the two-year simulation is shown in Fig. 11.

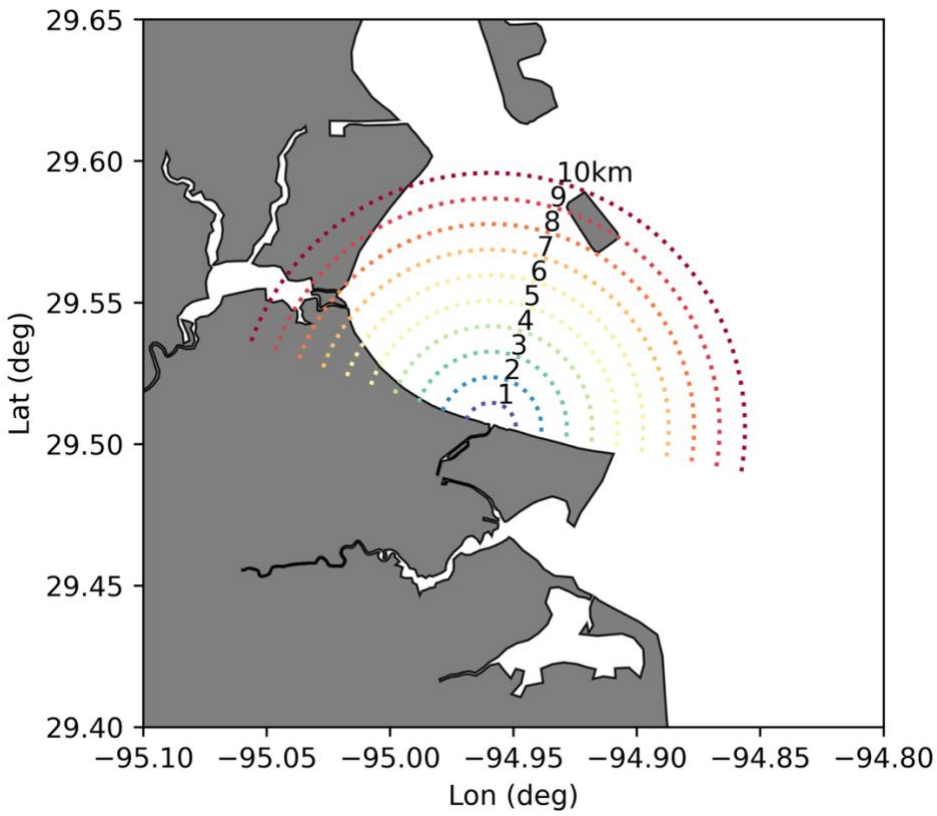


Figure 10: Regions within different radii (1–10 km) used for calculating regional mean salinity difference between the two model runs.

As expected, salinity increases are greater closer to the shoreline. For example, within a 1 km radius, the salinity increase can occasionally reach 1.25 ppt (Figs. 11 and Fig. 12). However, this level of increase is rare. On average, over the two-year period, the mean salinity increase within the 1 km radius is 0.12 ppt.

Interestingly, negative salinity impacts (i.e., scenario run salinity lower than base run) are also observed. In the latter half of the simulation (2019), multiple prolonged periods show negative salinity differences, such as between days 500–600. This occurs when the ambient salinity near the intake is significantly lower than that at the discharge site. As shown in Fig. 4, salinity at the intake (black line) and at the tidal dam (green line) are nearly identical under normal conditions. Since the brine has 147% of the intake salinity, it has higher salinity than the ambient discharge

location. However, for example, around day 500, the intake salinity drops to near 0 ppt, making the salinity of the discharged brine less than the surrounding bay water near the tidal dam. Effectively, the system behaves as though it is extracting freshwater from Dickinson Bay and releasing it near the shoreline—causing a local freshening.

This negative salinity impact accumulates. Starting around day 500, salinity differences decline sharply until day 530, then gradually increase. Similar negative events also occur around days 360, 600, and 700. These events are driven by differing hydrologic responses to freshwater pulses or rainfall in the small, enclosed Dickinson Bayou compared to the larger bay system. Small tidal creeks and bayous like Dickinson respond more sharply to precipitation events, leading to rapid salinity drops.

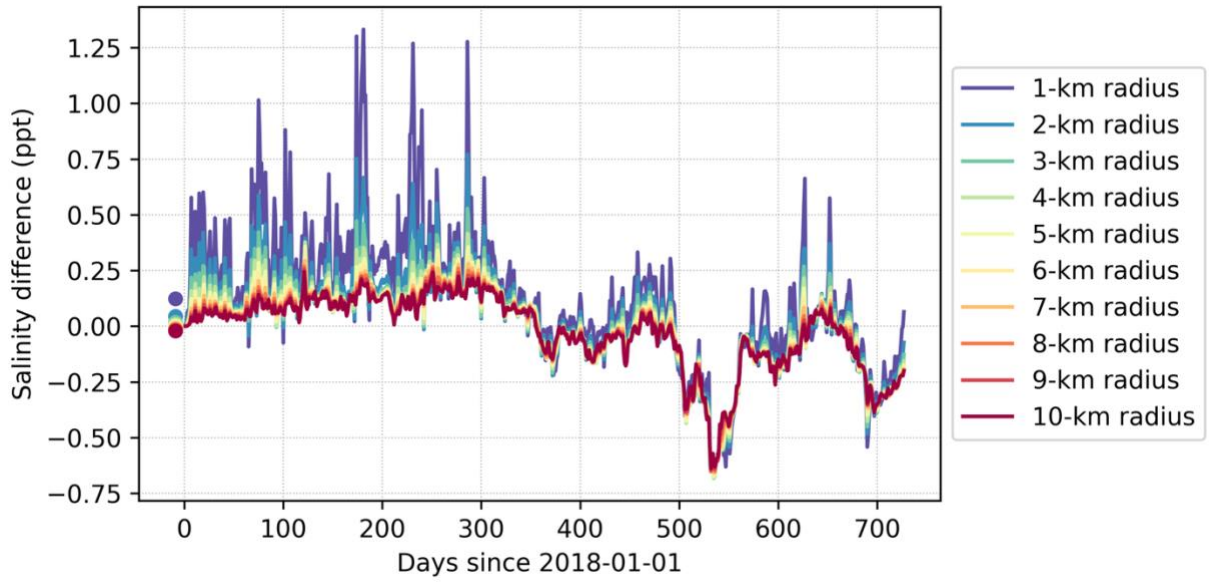


Figure 11: Time series of salinity difference (scenario minus base) averaged over different radii. Colored lines represent different averaging radii. Long-term mean differences are indicated by colored dots at the left of the plot.

To further understand the variability, we analyzed the distribution of regional salinity differences using violin plots. These plots display the maximum, minimum, median, and interquartile ranges. The median salinity difference decreases with distance—from the 1-km to the 10-km radius.

While most values are positive, negative impacts as large as −0.7 ppt are also seen. Notably, maximum positive impacts decline substantially with distance, whereas minimum (i.e., negative) impacts remain relatively consistent across radii.

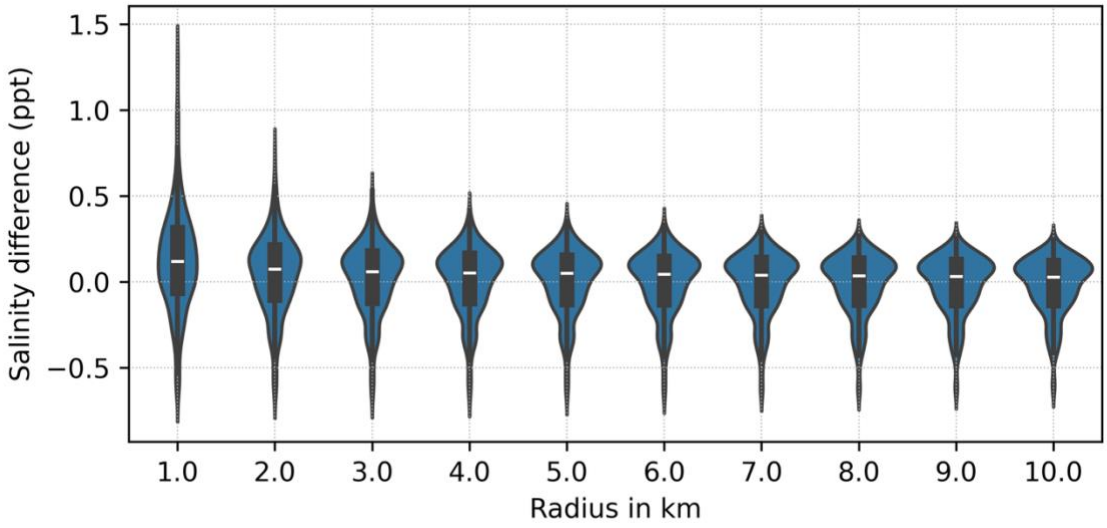


Figure 12: Violin plot showing the distribution of regional mean salinity differences due to brine discharge. The white bar marks the median, the black rectangle shows the interquartile range, the vertical line indicates the full range, and the outer shape illustrates the data distribution.

We also investigated finer-scale impacts using radii from 100 m to 1000 m (0.1–1 km), shown in Figs. 13 and Fig. 14. The pattern is consistent with the larger-radius analysis but with stronger impacts. For example, at a 100-m radius, salinity increases can reach up to 6 ppt.

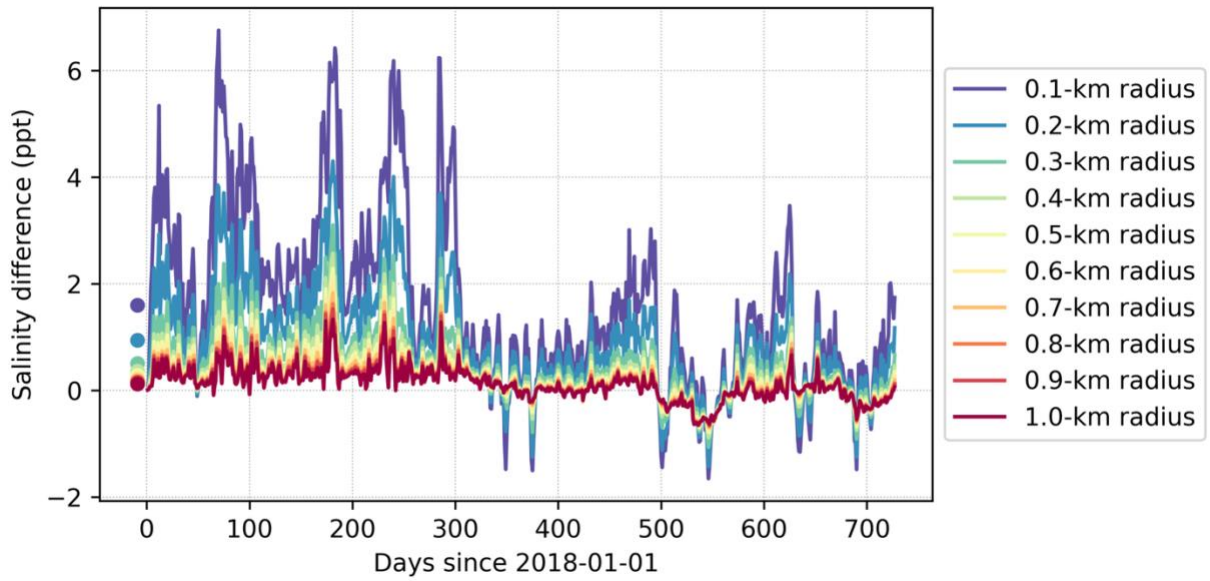


Figure 13: Same as Figure 11, but for smaller averaging radii from 100 m to 1 km.

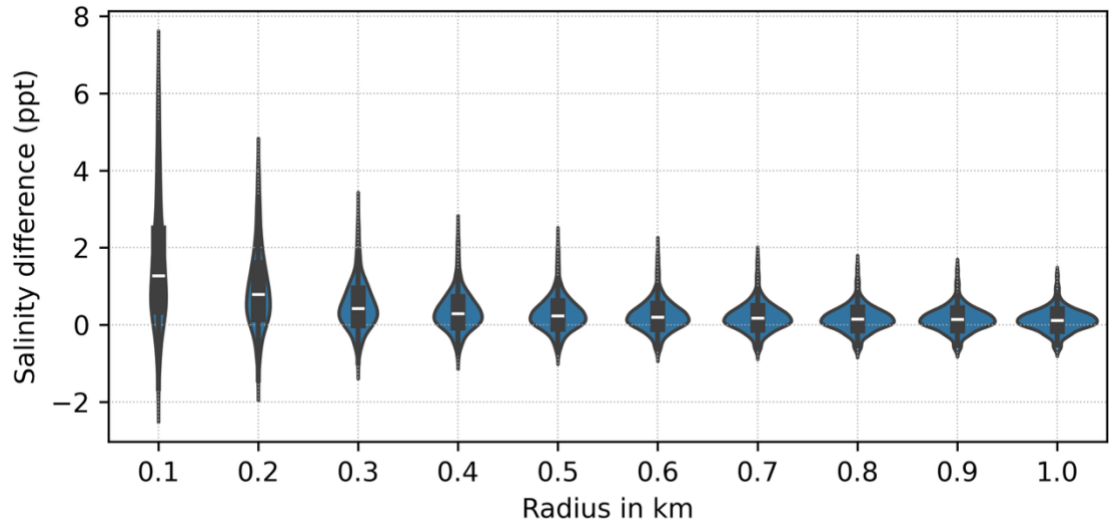


Figure 14: Same as Figure 12, but for smaller averaging radii from 100 m to 1 km.

Finally, Fig. 15 summarizes long-term mean salinity differences over various distances. As expected, the impact diminishes rapidly with distance from the discharge point. The mean salinity difference decreases from 0.12 ppt at 1 km to 0.04 ppt at 2 km. Beyond 5 km, negative salinity differences dominate due to the inclusion of parts of the lower bay where salinity tends to decrease (Fig. 7).

In conclusion, numerical experiments suggest a localized salinity increase near the brine outflow area, with the effect diminishing rapidly offshore. While increases up to 6 ppt can occur within 100 m, the long-term average impact is generally less than 0.2 ppt beyond 1 km, with some areas even experiencing slight salinity reductions.

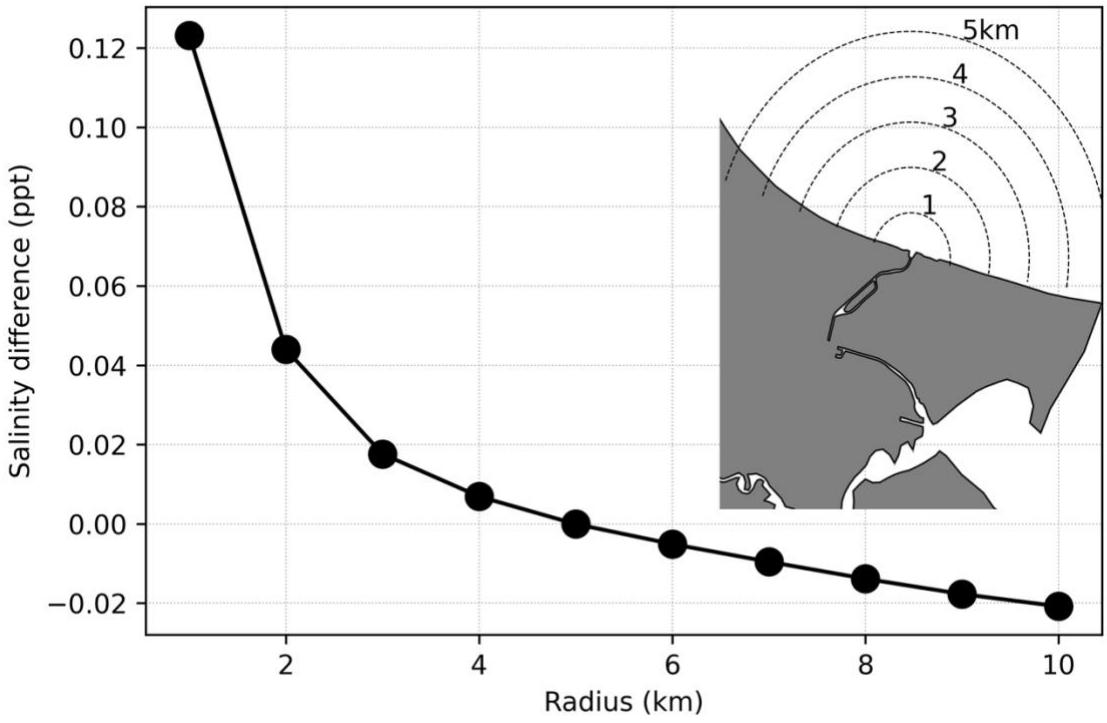


Figure 15: Long-term mean salinity difference averaged over the two-year period and over various radii. The inset at top right shows the 1–5 km radii used for regional averaging.

5. Impact of brine discharge on stratification

Brine discharge has higher salinity—and therefore higher density—than ambient bay water. As a result, discharged brine may enhance water column stratification by promoting denser water to settle near the bottom and move along the slope from the shoreline into the bay. Increased stratification can reduce vertical mixing, which may lead to lower bottom dissolved oxygen levels. This is of critical concern for benthic organisms that rely on adequate oxygen concentrations.

To assess this potential effect, we analyze the percentage of time with continuous stratification. Here, *continuous stratification* is defined as:

1) A surface-to-bottom salinity difference greater than 2 ppt, and
2) This condition must persist for at least 24 consecutive hours.

This index is commonly used to infer the risk of hypoxia, typically defined as bottom dissolved oxygen less than 2 mg/L. It is important to note that continuous stratification does not necessarily imply hypoxia, since bottom oxygen concentration also depends on surface temperature, biological oxygen demand, and total water depth. Also, the location of stratification matters. Areas that are close to the source of the brine tend to have higher DO due to recent formation of stratification and limited isolation time is available to deplete the bottom oxygen concentration to hypoxic levels. Furthermore, areas with significant bed slope can facilitate gravity flow of the brine. This movement entrains ambient waters into the brine, thereby diluting the brine and resupplying dissolved oxygen (Hodges, 2010). In Oso Bay, hypoxic events are typically found more than 1 km away from the brine source where the bottom topography is relatively flat and movement of the brine is limited (Hodges, 2010). Nevertheless, continuous stratification serves as a practical and interpretable proxy for identifying areas and periods with elevated hypoxia risk due to inhibited vertical mixing.

5.1 Percentage of time with continuous stratification

To quantify stratification over time, we follow the steps below for each grid point in the model domain:

1) Extract time series of surface and bottom salinity.
2) Compute the salinity difference between surface and bottom.
3) Identify periods when the salinity difference exceeds 2 ppt and persists for more than 24 hours.
4) Sum the duration beyond 24 hours of all such periods and divide by the total simulation time to obtain the percentage of time with continuous stratification.

The spatial distribution of this metric is shown in Fig. 16, for the base run, the scenario run (with brine discharge), and their difference. The overall pattern closely resembles the salinity difference, with a clear impact localized near the discharge region and negligible influence elsewhere in the bay.

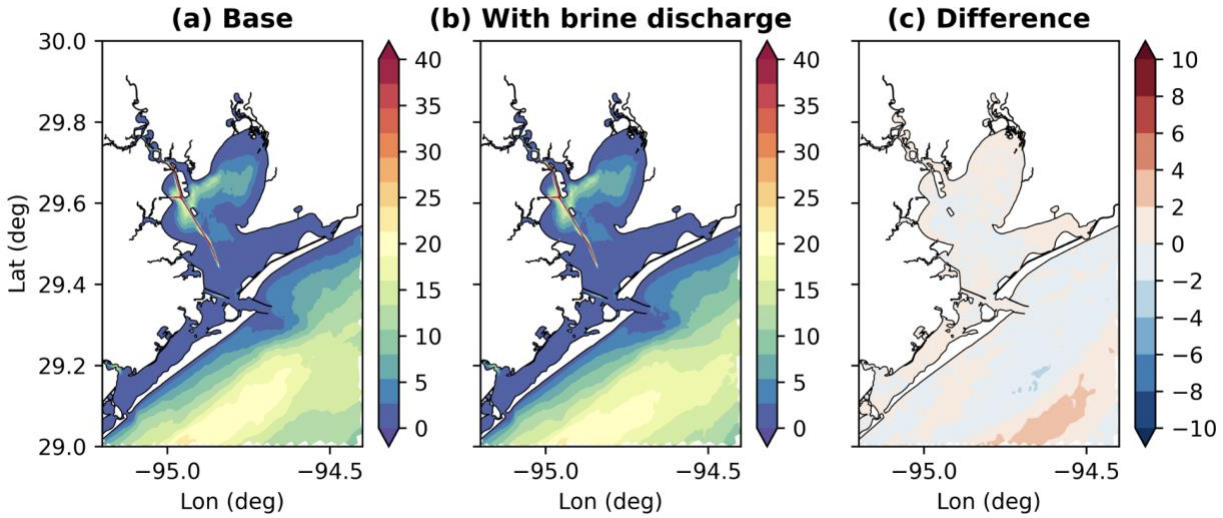


Figure 16: Percentage of time (%) when bottom–surface salinity difference exceeded 2 ppt for more than 24 hours. Left: base run; middle: scenario run; right: difference between the two, with positive values indicating a greater percentage in the scenario run.

A zoomed-in view (Fig. 17) highlights a substantial increase in the percentage of time with continuous stratification within a 1 km radius from the tidal dam, with increases reaching as high

as 30%. Beyond a 1 km radius, the effect becomes negligible, suggesting the stratification enhancement is strongly localized near the outflow channel.

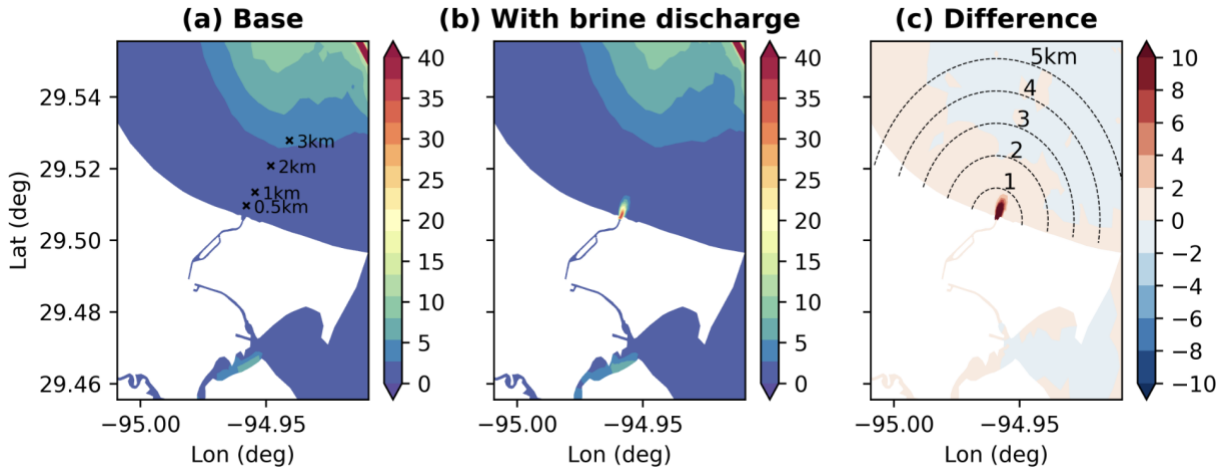


Figure 17: Same as Figure 16, but showing a zoomed-in view near the desalination plant. In (a), the cross marks indicate four sampling locations, at 0.5 km, 1 km, 2 km, and 3 km off the tidal dam. Time series of bottom-surface salinity difference at these two locations are shown in Figure 18 and Figure 21.

5.2 Time series at a selected location

We further examined the time series of stratification at two sampling locations located 0.5 km, 1 km, 2 km, and 3 km from the tidal dam, respectively. The results clearly indicate that stratification is strengthened in the brine discharge scenario, and the impact is much stronger at the nearshore location than at the offshore location. For the nearshore location 0.5 km off the tidal dam, the bottom-surface salinity difference could be as large as 8 ppt in the scenario run, compared to a maximum of 5 ppt in the base run. Impact on stratification at 1 km sampling location is still notable. Beyond 2 km off the tidal dam, the influence of brine discharge is negligible. At the offshore locations (e.g., 2 km and 3 km from the tidal dam), a strong increase of stratification also occurs, but it is not continuous throughout the simulation period. Instead, periods of enhanced stratification are intermittent.

It is essential to note that the elevated stratification in the nearshore region does not immediately imply a risk of hypoxia. The strong stratification in the nearshore region is primarily induced by higher-density brine water that tends to move downslope at the bottom under the influence of gravity, thereby increasing the bottom salinity. While the density flow has a larger salinity, it also carries a high concentration of dissolved oxygen. Furthermore, the nearshore region contains a sloping bottom portion where bottom elevation declines from 0 m NAVD88 at the tidal dam to -3 m NAVD88 at 1 km offshore. As mentioned earlier, the downslope movement of the density flow can cause DO entrainment, thereby reducing hypoxia risk. The current analysis can be refined further to conclude how brine discharge affects the dissolved oxygen condition in the nearshore region. We believe the nearshore region is unlikely to experience any hypoxia since the bay is shallow with a mean depth of 2.5 m and water can be easily mixed. A follow-up modeling effort using a fully coupled physical-biogeochemical model can help assess the impact on dissolved oxygen more thoroughly.

The frequency and duration of stratified events are notably reduced in 2019 compared to 2018. This observation is consistent with the previously discussed salinity impacts, which showed smaller or even negative differences in 2019 due to varying freshwater inputs and ambient conditions near the intake and discharge locations. These results reinforce the conclusion that the strength and duration of brine-induced stratification depend heavily on background hydrological and meteorological conditions.

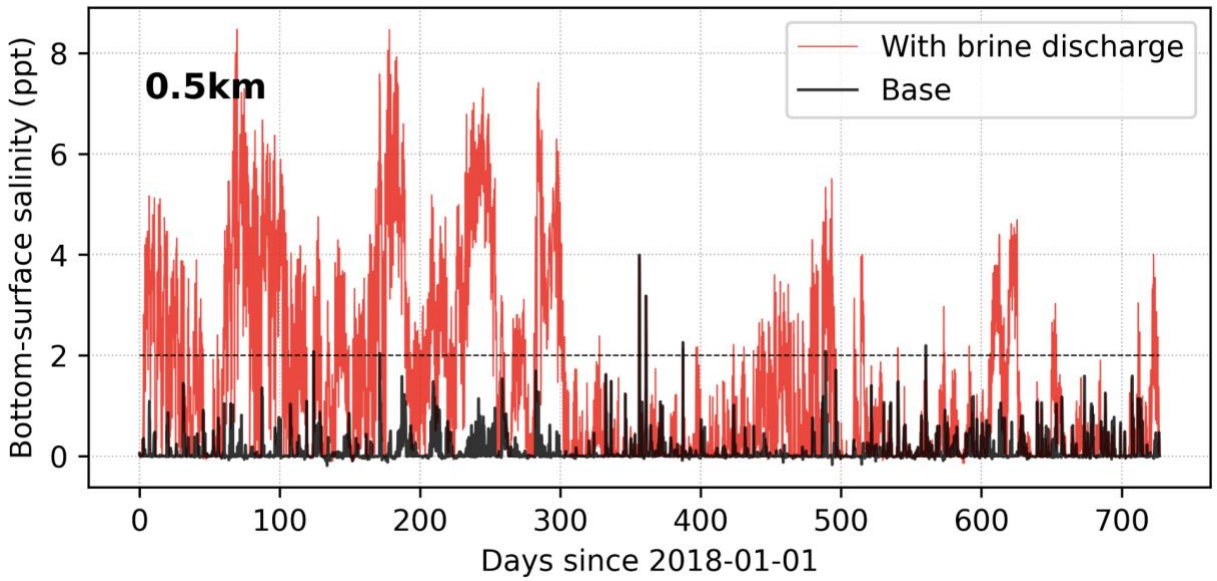


Figure 18: Time series of bottom–surface salinity difference at a sampling location 0.5 km offshore from the tidal dam near the desalination plant.

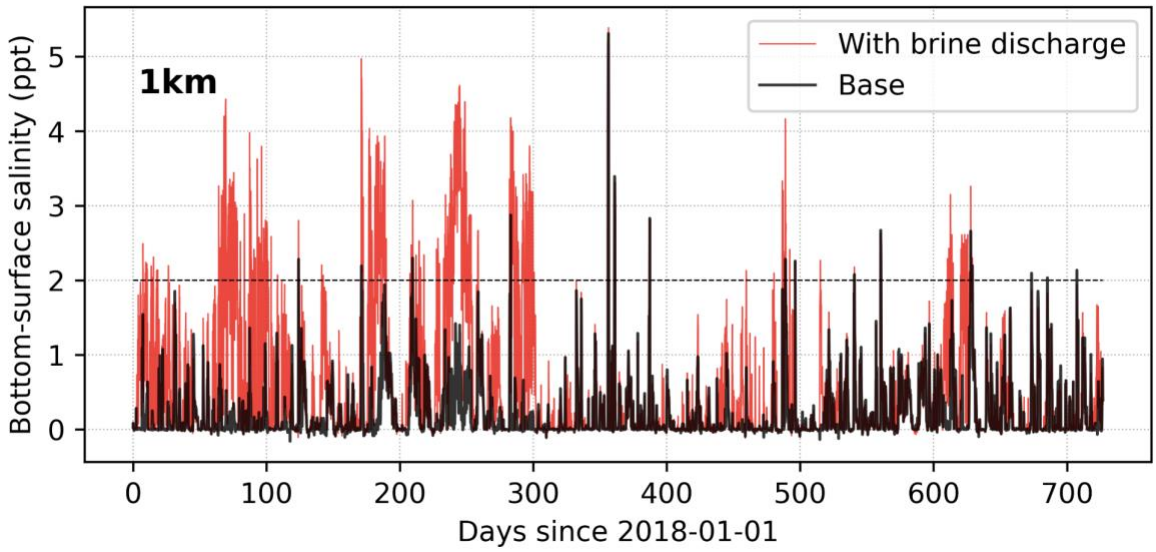


Figure 19: Time series of bottom–surface salinity difference at a sampling location 1 km offshore from the tidal dam near the desalination plant.

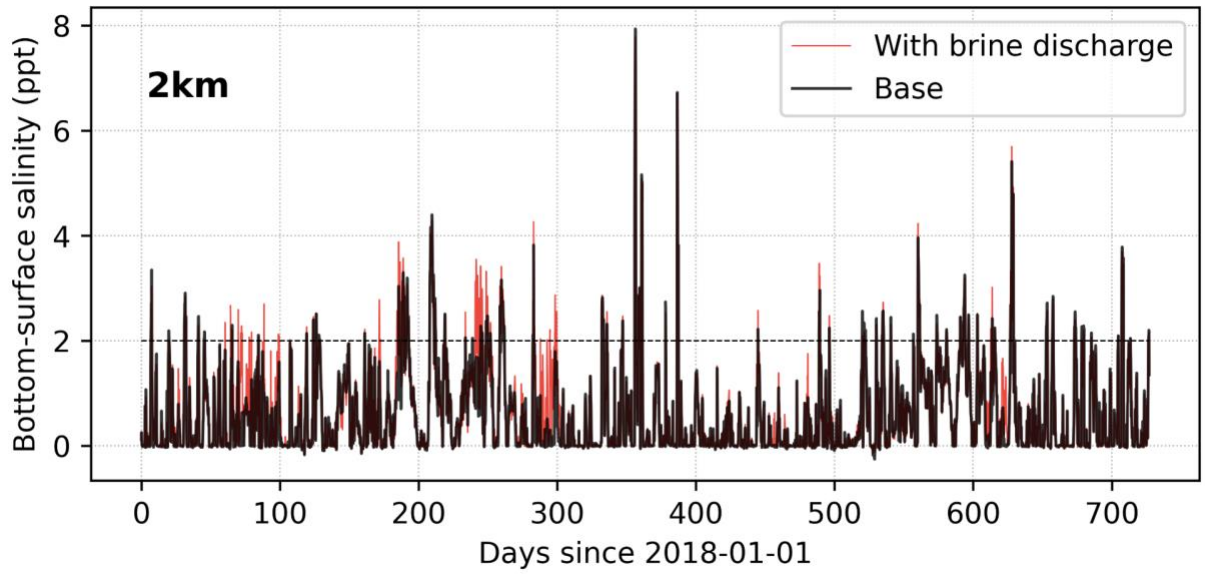


Figure 20: Time series of bottom–surface salinity difference at a sampling location 2 km offshore from the tidal dam near the desalination plant.

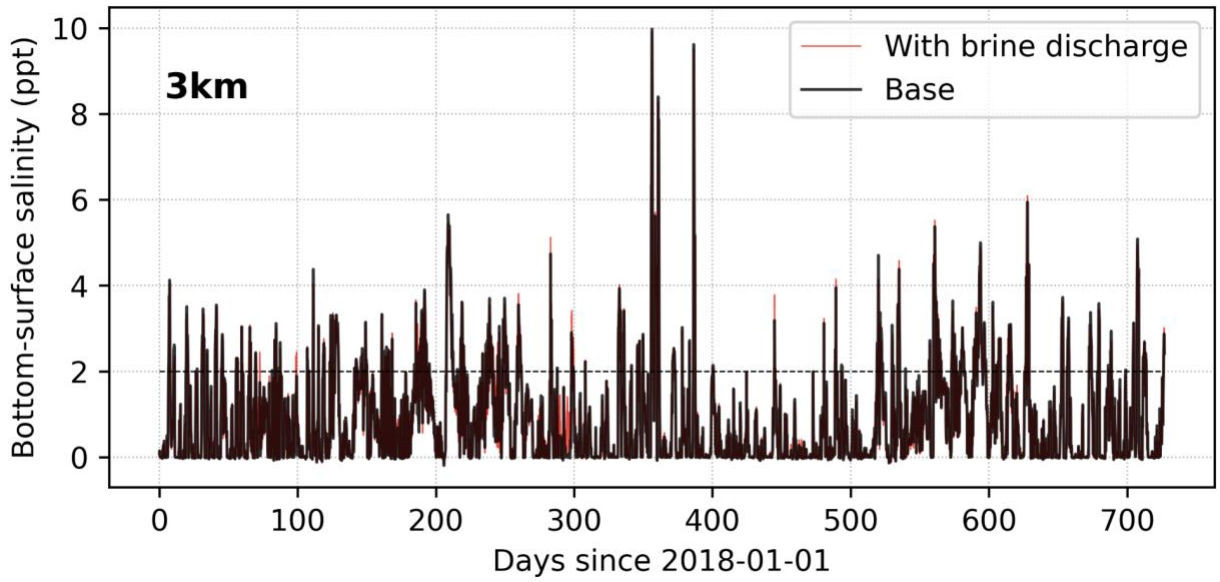


Figure 21: Time series of bottom–surface salinity difference at a sampling location 3 km offshore from the tidal dam near the desalination plant.

6. Discussion and summary

Using a validated and reliable ocean model, this study assessed the impact of brine water discharge from a proposed desalination plant in Galveston Bay. Two model scenarios were compared: one without any intake or discharge and another with seawater intake of 82.8 million gallons per day (MGD) from Dickinson Bayou and discharge of 56.3 MGD of diluted brine water. Results indicate that the salinity impact is spatially limited, primarily confined to the vicinity of the outflow location.

Within 1 km of the tidal dam that connects the discharge channel to the bay, the mean surface salinity increases by approximately **0.12 ppt**, and the impact diminishes rapidly offshore. Within the discharge channel itself, salinity can increase by up to 5 ppt. This relatively modest effect is due to the discharge rate, which corresponds to only 2.96 m^3/s.

The intake/discharge scheme can also be interpreted as a net reduction of approximately 26.5 MGD (or 1.39 m^3/s) of freshwater to the system. When compared to the total freshwater inflow into Galveston Bay—typically ~300 m^3/s from the San Jacinto River, Trinity River, and Buffalo Bayou (Marshall and Montagna, 2025) —this reduction is unlikely to significantly alter bay-wide salinity patterns.

A notable and somewhat unexpected finding is that the salinity impact is more pronounced near the intake channel than near the discharge location. Using a threshold of 0.1 ppt, the impact region around the intake extends farther than that near the discharge. This is physically reasonable: the intake acts as a localized “sink,” drawing additional seawater into Dickinson Bayou to compensate for water extraction, which leads to elevated salinity along the bayou.

Another important insight is that the salinity impact can be negative, depending on the difference between the intake salinity and the ambient salinity at the discharge location. For example, when freshwater inflow significantly reduces intake salinity (e.g., near 0 ppt), the discharged brine may be less saline than nearby bay water, thereby reducing salinity at the discharge site.

With regard to stratification and potential hypoxia risk, we found that brine discharge can substantially increase the percentage of time with continuous stratification (defined as surface-bottom salinity difference > 2 ppt sustained for over 24 hours) in the nearshore region. Within 1 km of the tidal dam, the percentage of time with stratification can increase by up to 30%. However, this elevated stratification in the nearshore is primarily induced by density flow as the denser brine water moves downslope at the bottom. It is challenging to determine how elevated nearshore stratification affects dissolved oxygen, as the brine water also contains a high concentration of dissolved oxygen and that downslope movement can also entrain ambient waters and resupply dissolved oxygen. Impact on nearshore dissolved oxygen needs to be further assessed with a fully coupled physical biogeochemical modeling system. However, we believe the brine discharge is unlikely to impact dissolved oxygen beyond 1 km off the tidal dam, as the impact on stratification also diminishes quickly with distance from shore and is generally negligible beyond 2 km from the tidal dam.

Summary from numerical experiments

1) The proposed intake and discharge scheme has a localized and relatively small salinity impact, generally less than 1 ppt in both intake and discharge regions.
2) The system's response is sensitive to background hydrology; for example, the salinity impact is reduced or even negative under wet conditions.

Limitations of this study

It is important to note several limitations of the present study, including:

1) The simulation period only covers two years (2018–2019). It does not include extreme drought or wet years. We selected these two years as the hydrodynamic simulation have been well validated and the base simulation (without discharge) has been used in several studies (e.g., Summers et al., 2024; Hua et al. 2025)
2) We assume the tidal dam does not exist and that there is no elevated bathymetry at the dam, as information on how the tidal dam operates is lacking. The tidal dam has an elevation close to 0 meter at datum of NAVD 88 (i.e., close to mean sea level), meaning

bay water would only enter the discharge channel when the sea level is higher than the mean sea level. In this case, tidal mixing in the outflow channel would be less than an open channel without a dam, potentially leading to the accumulation of brine water in the discharge channel. If feasible, it may be better to remove the dam, allowing bay water to enter the discharge channel freely. The impact of the tidal dam needs further evaluation.

3) The impact of future conditions, such as sea level rise, should be considered, as sea level rise will affect the transport and mixing of salt, as well as the exchange between bay water and ocean water.

References

Carrere, L., Lyard, F., Cancet, M., and Guillot, A. (2015): FES 2014, a new tidal model on the global ocean with enhanced accuracy in shallow seas and in the Arctic region, in: Abstracts of the EGU General Assembly 2015, Vienna, Austria, 12–17 April 2015. http://adsabs.harvard.edu/abs/2015EGUGA..17.5481C

Chen, X., Liu, C., O'Driscoll, K., Mayer, B., Su, J., & Pohlmann, T. (2013). On the nudging terms at open boundaries in regional ocean models. *Ocean Modelling*, *66*, 14–25. https://doi.org/10.1016/j.ocemod.2013.02.006

Du, J., & Park, K. (2019). Estuarine salinity recovery from an extreme precipitation event: Hurricane Harvey in Galveston Bay. *Science of The Total Environment*, *670*, 1049–1059. https://doi.org/10.1016/j.scitotenv.2019.03.265

Du, J., Shen, J., Zhang, Y. J., Ye, F., Liu, Z., Wang, Z., et al. (2018). Tidal response to sea-level rise in different types of estuaries: The importance of length, bathymetry, and geometry. *Geophysical Research Letters*, *45*(1), 227–235. https://doi.org/10.1002/2017GL075963

Du, J., Park, K., Shen, J., Zhang, Y. J., Yu, X., Ye, F., et al. (2019). A hydrodynamic model for Galveston Bay and the shelf in the northern Gulf of Mexico. *Ocean Science*, *15*(4), 951–966. https://doi.org/10.5194/os-15-951-2019

Du, J., Park, K., Yu, X., Zhang, Y. J., & Ye, F. (2020). Massive pollutants released to Galveston Bay during Hurricane Harvey: Understanding their retention and pathway using Lagrangian numerical simulations. *Science of the Total Environment*, 704, 135364. https://doi.org/10.1016/j.scitotenv.2019.135364

Hua, J., Du, J., & Park, K. (2025). Shelf-wide circulation impacts the flushing time of coastal bays. Ocean Modelling, 102603. https://doi.org/10.1016/j.ocemod.2025.102603

Hodges, B.R., 2010, The importance of mixing and isolation time for desalination brine discharge, International Engineering Conference on Hot Arid Regions (IECHAR 2010) Al-Ahsa, KSA, March 1-2, 2010

Kantha, L. H., & Clayson, C. A. (1994). An improved mixed layer model for geophysical applications. *Journal of Geophysical Research*, 99(C12), 25235–25266. https://doi.org/10.1029/94JC02257

Marshall, D. A., & Montagna, P. A. (2025). Nitrogen and phosphorus budgets for Texas estuaries. In *Freshwater inflows to Texas Bays and Estuaries* (edited by P.A. Montagna & A.R. Douglas), Springer. pp 363-388.

Summers, E., Du, J., Park, K., & Kaiser, K. (2023). How does buoyancy behavior impact microplastic transport in an estuarine environment? *Science of The Total Environment*, *899*, 165687. https://doi.org/10.1016/j.scitotenv.2023.165687

Summers, E., Du, J., Park, K., & Kaiser, K. (2024). Quantifying the Connectivity of Microplastic Pollution in the Texas–Louisiana Coastal Area. *CS EST Water*, 4 (6), 2482–2494. https://doi.org/10.1021/acsestwater.3c00839

Umlauf, L., & Burchard, H. (2003). A generic length-scale equation for geophysical turbulence models. *Journal of Marine Research*, 61(2), 235–265. https://doi.org/10.1357/002224003322005087

Ye, F., Zhang, Y. J., Wang, H. V., Friedrichs, M. A. M., Irby, I. D., Alteljevich, E., et al. (2018). A 3D unstructured-grid model for Chesapeake Bay: Importance of bathymetry. *Ocean Modelling*, *127*, 16–39. https://doi.org/10.1016/j.ocemod.2018.05.002

Ye, F., Zhang, Y. J., Yu, H., Sun, W., Moghimi, S., Myers, E., et al. (2020). Simulating storm surge and compound flooding events with a creek-to-ocean model: Importance of baroclinic effects. *Ocean Modelling*, *145*, 101526. https://doi.org/10.1016/j.ocemod.2019.101526

Zhang, Y., & Baptista, A. M. (2008). SELFE: A semi-implicit Eulerian–Lagrangian finite-element model for cross-scale ocean circulation. *Ocean Modelling*, *21*(3), 71–96. https://doi.org/10.1016/j.ocemod.2007.11.005

Zhang, Y. J., Ateljevich, E., Yu, H. C., Wu, C. H., & Yu, J. C. S. (2015). A new vertical coordinate system for a 3D unstructured-grid model. *Ocean Modelling*, *85*, 16–31. https://doi.org/10.1016/j.ocemod.2014.10.003

Zhang, Y. J., Ye, F., Stanev, E. V., & Grashorn, S. (2016). Seamless cross-scale modeling with SCHISM. *Ocean Modelling*, *102*, 64–81. https://doi.org/10.1016/j.ocemod.2016.05.002